Energy Measurement of X-rays in Computed Tomography for Detecting Contrast Media

Ikuo KANNO , Akio UESAKA , Seiichiro NOMIYA & Hideaki ONABE

ARTICLE

Energy Measurement of X-rays in Computed Tomography for Detecting Contrast Media

Ikuo KANNO[1,*], Akio UESAKA[1], Seiichiro NOMIYA[2] and Hideaki ONABE[2]

[1]*Graduate School of Engineering, Kyoto University, Sakyo, Kyoto 606-8501, Japan*
[2]*Raytech Corporation, Yoto, Utsunomiya 321-0904, Japan*

The advantages of energy measurement of x-rays over current measurement in transmission radiography and computed tomography (CT) for detecting iodine contrast media are discussed. Simulation studies on both methods of measurement are carried out, followed by experiments. As data for energy measurement of x-rays, the event ratio of two energy regions with a K-edge of iodine between them is employed. The energy measurement method is immune to beam hardening, while current measurement suffers greatly with changes in x-ray tube voltage and thickness of the body under measurement. This method is useful in interventional radiology and in CT. It will also be useful for detecting other types of contrast medium.

KEYWORDS: x-ray, energy subtraction, transmission measurement, CT, contrast media, beam hardening

I. Introduction

In x-ray transmission radiography and x-ray computed tomography (CT), iodine contrast media are sometimes employed to make tumors such as cancers observable. X-ray CT is one of the most powerful tools for determining cancers. The dose exposure with CT measurement, however, is some 10 to 1,000 times higher than that with normal chest radiography. The reduction of the dose exposure with CT measurement needs to be intensively studied to reduce the amount.

For the reduction of the dose exposure on x-ray transmission radiography and x-ray CT, we proposed a method called the filtered x-ray energy subtraction method (FIX-ES).[1] In this method, unnecessary x-rays, in other words, x-rays that are not very sensitive to iodine, are cut out by a filter, which is constructed from an element, *e.g.*, lanthanum, with slightly higher atomic number than iodine. The energy of individual x-rays is measured and the numbers of events in fixed energy ranges are employed as energy information. This method is radically different from the conventional one, which measures x-rays as current.

With using FIX-ES, the dose exposure was reduced to 30% with the choice of the filter thickness; that is, a 70% reduction.[1,2] In the comparison between the current measurement and FIX-ES in transmission radiography, FIX-ES was found to have a sensitivity that was two times better than that of the current measurement.[3]

Other energy subtraction (ES) methods have been proposed; however, most measured x-rays as current,[4–8] with the exception of bone mineral measurements in which two energy windows were employed with the ES method.[9,10] No ES method, however, has been dedicated to the reduction of dose exposure. Although FIX-ES is a promising method for detecting iodine contrast media, it is not practically employed, mainly because x-ray detectors with a high counting rate that would be used in practical CT measurements are not yet available.

Putting aside for future study the unavailability of x-ray energy detectors with a high counting rate, we discuss the advantages of energy measurements of x-rays in CT in this paper. In the current measurements of x-rays, the effect of iodine contrast media changes because of the physical size of the body being examined and the accelerating voltage of the x-ray tube, *i.e.*, changes in the x-ray energy spectrum. Because of these characteristics, a cancer in a large patient could be harder to determine than one of the same size but in a thin patient.

In this paper, we present a comparison between the current and FIX-ES measurement methods of x-rays in CT. We present the results of a simulation study for detecting iodine contrast media in simple phantoms, followed by the experimental results of CT measurements.

II. Comparison of Current and Energy Measurement Methods

In earlier studies, we used the FIX-ES method to estimate the iodine thickness in a cancer tissue of 10 mm thickness in the direction of an x-ray source to an x-ray detector.[1–3] This estimation was performed for cancer tissue with iodine, but

not for normal tissue. That is, we did not take into account the appearance of cancer tissue with iodine when observed surrounded by normal tissue. In this section, we first theoretically describe the FIX-ES method, followed by simulation study for detecting the iodine region in a water phantom, and then by experimental results obtained using a simple phantom.

1. Estimation of Iodine Thickness

A typical contrast medium contains 30–32 g of iodine in 100–150 ml.[11] For simplicity, in the present study, we consider 30 g of iodine in 100 ml of contrast medium to be injected into a typical patient of 60 kg weight and 6,000 ml blood volume.

Two important assumptions were made regarding the iodine distribution: (1) the contrast medium is uniformly diluted in the 6,000 ml of blood, and (2) the contrast medium is not diluted by blood and retains its iodine concentration as it moves through the blood vessels.[12] Thus, the iodine concentrations for cases (1) and (2) are 5 and 300 mg/ml, respectively. In the case of a cancer tissue of 10 mm thickness, the iodine thicknesses for cases (1) and (2) would be 10 and 600 μm, respectively, using an iodine density of nearly 5 g cm^{-3}. When we assume that the portion of blood vessel in a cancer is 10%, which is the same as that for normal tissue but is employed for the purpose of underestimating the iodine thickness, the iodine thickness to be detected is 1–60 μm in a 10-mm-thick cancer tissue.

Another way of estimating iodine thickness is that the iodine is entirely diluted in the human body of 60 kg weight, *i.e.*, 60 L of water. The iodine density in this case is 0.5 mg/ml. As a result, the iodine thickness in 10 mm of nor-

mal tissue is 1 μm. Considered this way, the iodine thickness in a cancer tissue could be assumed to be thicker than 1 μm.

2. Theoretical Prediction

The energy spectrum of x-rays, $\Psi_0(E)$, emitted by the bombardment of electrons with acceleration voltage E_0 to a target such as tungsten is generally described by the following equation[13]

$$\Psi_0(E)dE = const. \times Z \frac{E_0 - E}{E} dE, \quad (1)$$

where Z is the atomic number of the target and E is the energy of the x-rays. With absorbers between the x-ray source and the x-ray detector, the measured x-ray spectrum $\Psi(E)$ is given as

$$\Psi(E)dE = \Psi_0(E) \cdot \exp\left\{-\sum_i (\mu_i/\rho_i \times t_i \times \rho_i)\right\} dE, \quad (2)$$

where μ_i/ρ_i is the mass attenuation coefficient, t_i is the thickness, and ρ_i is the density of material i. There is good agreement between the calculation results obtained using this equation and experimental results, as shown in Fig. 3 of Ref. 1).

As described in Refs. 1–3), numbers of x-ray events ϕ_1, ϕ_2, in two energy regions E_1 (27.4–33.2 keV), E_2 (33.2–38.9 keV), respectively, were employed for the evaluation of iodine thickness by the FIX-ES method. The energies of 33.2 and 38.9 keV correspond to the ones of the K-edges of iodine and lanthanum, respectively. The number of x-rays after summing up all the energy after passing through the cancer with iodine is found by the following equation,

$$\phi = \sum_n \Psi(E_n) \cdot \exp\{-\mu_I(E_n) \cdot t_I\} \cdot \exp\{-\mu_W(E_n) \cdot t_W\}. \quad (3)$$

Here, $\mu_I(E_n)$ and $\mu_W(E_n)$ are the x-ray attenuation coefficients of iodine and water, respectively, for x-rays with energy E_n. The energy E_n corresponds to the one of an x-ray measured in channel number n of a multichannel analyzer. The thicknesses of iodine and water are assigned as t_I and t_W, respectively. $\Psi(E_n)$ is the number of x-rays with energy E_n before entering the body being examined. If we define averaged absorption coefficients of iodine and water for the energy regions of E_i ($i = 1, 2$) as $\overline{\mu_I}(E_i)$ and $\overline{\mu_W}(E_i)$, respectively, Eq. (3) is rewritten as

$$\phi_i = \Psi(E_i) \cdot \exp\{-\overline{\mu_I}(E_i) \cdot t_I\} \cdot \exp\{-\overline{\mu_W}(E_i) \cdot t_W\}. \quad (4)$$

For CT measurements by the FIX-ES method, we propose the ratio ϕ_1/ϕ_2 for CT data. The ratio ϕ_1/ϕ_2 is written as

$$\frac{\phi_1}{\phi_2} = \frac{\Psi(E_1)}{\Psi(E_2)} \exp\{-(\overline{\mu_I}(E_1) - \overline{\mu_I}(E_2)) \cdot t_I\} \cdot \exp\{-(\overline{\mu_W}(E_1) - \overline{\mu_W}(E_2)) \cdot t_W\}. \quad (5)$$

The logarithm of ϕ_1/ϕ_2 is obtained as

$$\ln \frac{\phi_1}{\phi_2} = \ln\left\{\frac{\Psi(E_1)}{\Psi(E_2)}\right\} - (\overline{\mu_I}(E_1) - \overline{\mu_I}(E_2)) \cdot t_I - (\overline{\mu_W}(E_1) - \overline{\mu_W}(E_2)) \cdot t_W. \quad (6)$$

In CT measurements, data at a point without the body being examined, *i.e.*, no iodine or water but just air, should be measured as well as the body. When the result in the air region is normalized to unity, Eq. (6) is rewritten as

$$\ln \frac{\phi_1}{\phi_2} = 1 - (\overline{\mu_I}(E_1) - \overline{\mu_I}(E_2)) \cdot t_I - (\overline{\mu_W}(E_1) - \overline{\mu_W}(E_2)) \cdot t_W. \quad (7)$$

Equation (7) shows the reason why FIX-ES measurements are not influenced by the energy spectrum of x-rays.
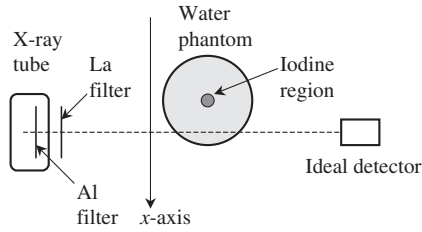
Fig. 1   Geometry of the calculation used in the simulation of x-ray transmission measurements.

3. Simulation Study

The geometry of the calculation is shown in **Fig. 1**. The x-ray tube has a built-in 2-mm-thick Al filter, with a 100-μm-thick lanthanum filter attached as an additional filter. A cylindrical water phantom is placed between the x-ray source and an ideal x-ray detector. Calculations were performed with the diameters of the water phantom taken as 100, 200, and 300 mm. The iodine region was defined as being 10 mm in diameter at the center of the water phantom. The water phantom moved along the x-axis with a step of 0.5 mm, and the thicknesses of water and iodine were calculated as a function of the x-position of the phantom. X-ray energy spectra were obtained as a function of the x-position of the phantom using Eq. (2). These spectra correspond to the results of energy measurements in x-ray transmission measurements. The calculation code for the simulation study was developed by the authors.

Figure 2 shows the calculated x-ray energy spectra as a function of iodine thickness using tube voltages of 50, 65, and 80 kV for the case of a water thickness of 200 mm. Characteristic x-rays of tungsten are not taken into account in this calculation. The energy bin used in the calculation was 1 keV. The current I for these energy spectra was calculated as

$$I \propto \sum_n Y(E_n) \times E_n, \tag{8}$$

where $Y(E_n)$ is the number of x-rays with energy E_n. By using this calculation, a comparison could be performed between energy and current measurements under the same dose exposure conditions. This condition is hardly achieved in practice, because the numbers of x-rays required for current and energy detectors are different by some orders of magnitude.

In the energy measurement, the summed events ϕ_1 and ϕ_2 of the two energy regions E_1 (27–32 keV) and E_2 (33–38 keV), respectively, are obtained and the ratio ϕ_1/ϕ_2 is employed according to the FIX-ES method. As noted above, the energies of 33 and 38 keV correspond to the K-edges of iodine and lanthanum, respectively. The results of current measurement and FIX-ES measurement for simulated x-ray transmission images are shown in **Figs. 3** and **4** for water phantom diameters of 200 and 300 mm, respectively, and x-ray tube voltages of 50, 65, and 80 kV.

To investigate the effect of lanthanum filter thickness, the same calculations were repeated with 0-, 100-, and 200-μm-thick lanthanum filters. The differences in relative current
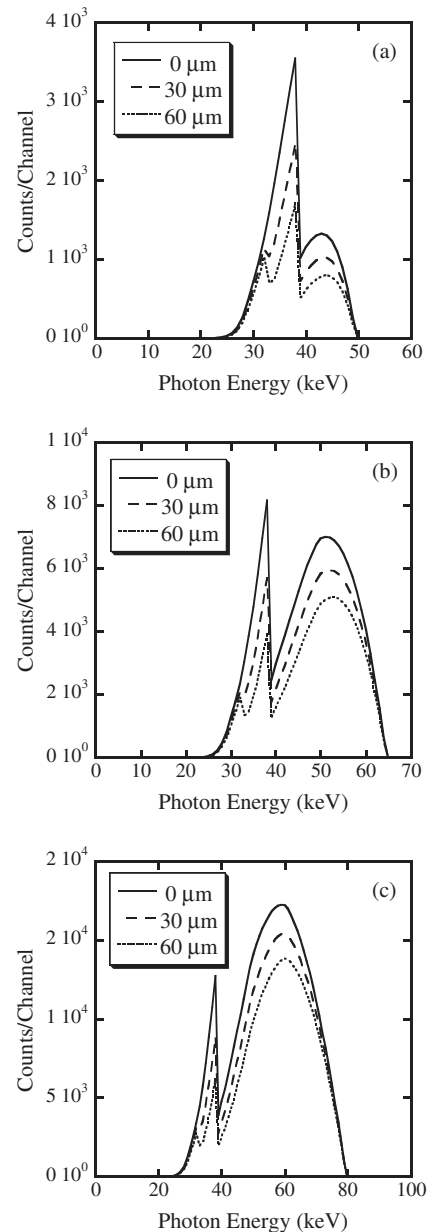
Fig. 2   X-ray energy spectra after transmission through an Al filter (2 mm), lanthanum filter (100 μm), and water phantom (200 mm) for iodine regions of 10 mm thickness. The x-ray tube voltages are (a) 50, (b) 65, and (c) 80 kV. The thicknesses of iodine in a 10-mm-thick water layer are also shown.

and relative ϕ_1/ϕ_2 between the iodine thicknesses of 0 and 60 μm were then calculated (Fig. 5). In calculating current, the differences changed according to the x-ray tube voltage, whereas in calculating ϕ_1/ϕ_2, the x-ray tube voltage had no effect as shown in **Fig. 5**. No significant dependence on lanthanum filter thickness was observed in either calculation.

To convert the results of x-ray transmission measurements into CT measurements, the data set of the x-axis scan was repeated 60 times as angle-scanned data with a step of 3°; because the phantom has axial symmetry, the x-scanned data alone provide sufficient raw data for CT measurement. **Figure 6** shows CT images for current measurement and FIX-ES measurement in the case of a water phantom of
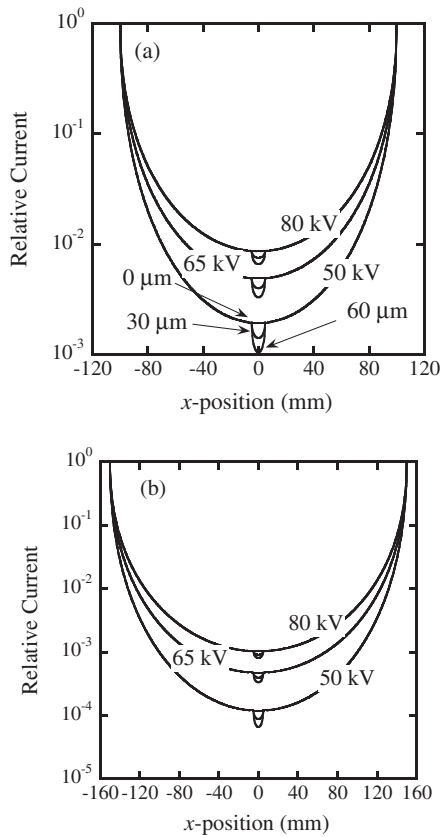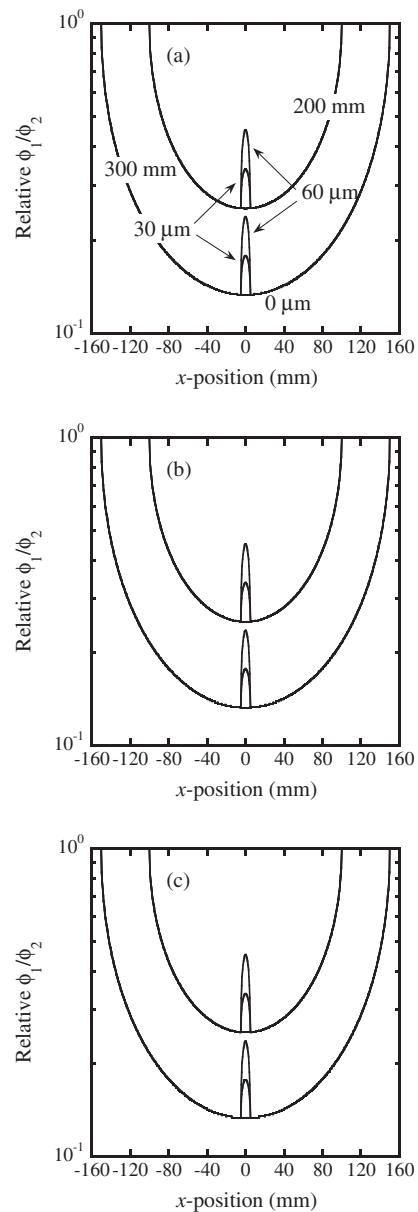
Fig. 3 Calculation results of the relative currents obtained in the simulation described in Fig. 1 are shown for the cases of phantom diameters of (a) 200 and (b) 300 mm. The x-ray tube voltages and the iodine thicknesses in the 10-mm-thick water layer are indicated in the figure.


Fig. 4 Calculation results of relative ϕ_1/ϕ_2 obtained in the simulation described in Fig. 1 for x-ray tube voltages of (a) 50, (b) 65, and (c) 80 kV. The diameter of the phantom and the iodine thickness in the 10-mm-thick water layer are shown in the figure.

200 mm diameter, iodine thickness of 60 μm in 10-mm-thick water layer, x-ray tube voltage of 65 kV, and a lanthanum filter of 100 μm thickness. The CT images are not easily discussed quantitatively; therefore, the profiles at the center line of each CT image are shown in **Fig. 7** for the case of the water phantom of 200 mm diameter and for x-ray tube voltages of (a) 50, (b) 65, and (c) 80 kV. The value of the *y*-axis is termed the CT value; this term is applied as it is commonly used in CT images in the conventional current measurement method. **Figure 8** shows comparisons made for water phantoms with diameters of (a) 100 and (b) 300 mm with 65 kV tube voltage. In Figs. 7 and 8, the iodine thicknesses are shown as 0, 30, and 60 μm, respectively, in a 10-mm-thick water layer.

4. Experimental Study

We employed a simple phantom to confirm the validity of the simulation study. The experimental setup was similar to that shown in Fig. 1, although with the following differences. An acryl cylinder phantom of 30 mm diameter was used instead of the cylindrical water phantom. A hole of 10 mm diameter was bored in the center of the acryl cylinder phantom, and water-thinned iodine tincture was installed into the hole. A water layer of 200 mm thickness was placed between the acryl cylinder phantom and the x-ray detector

to reduce the number of x-rays and thus avoid dead time of the x-ray detector during energy measurements.

An acryl phantom of 30 mm diameter was employed to reduce the measurement time. For comparison with the calculation described above, a phantom of 200 mm diameter might appear to be reasonable; however, nothing happens apart from the absorption of x-rays by the acryl by changing its thickness before the center of the phantom reaches the x-ray tube detector line. The additional water layer of 200 mm thickness enables us to obtain an x-ray energy spectrum that is similar to the one in the calculation study. The x-ray absorption behavior of acryl is similar to that of water.

The x-ray source was UD-150B (Shimadzu Corp.) with a built-in 2-mm-thick Al filter. A CdZnTe (CZT) detector
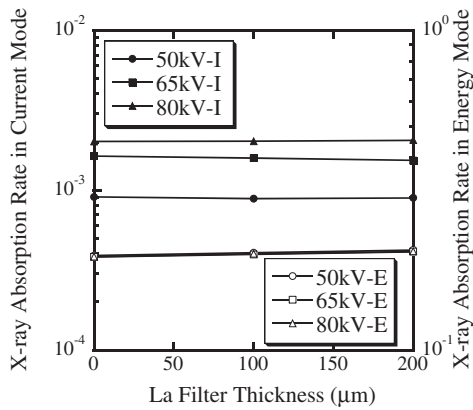
Fig. 5 The effect of lanthanum filter thickness on the relative current and relative ϕ_1/ϕ_2. The absolute values of the difference in current (left y-axis) and ϕ_1/ϕ_2 (right y-axis) are shown for iodine thicknesses of 0 and 60 µm. The x-ray tube voltages are also shown. "I" and "E" represent current and ϕ_1/ϕ_2 calculations, respectively. The thickness of the water phantom was 200 mm.

(Amptek XR-100T-CZT) was used as the x-ray detector. The CZT crystal dimensions were $3 \times 3 \times 2$ mm³; the crystal was cooled to $-20°C$ using a Peltier cooler. The applied bias voltage was 400 V. The x-rays were collimated by lead plates of 2 mm thickness; the collimation was 2 mm at the x-ray tube and 0.5 mm at the CZT detector. The obtained x-ray energy spectra suffered distortion caused by the escape of x-rays from the relatively small CZT crystal; the distortion was corrected via a stripping method.[2,14]

By assigning the line that connected the x-ray tube and the CZT detector as $x = 0$, the acrylic phantom was moved from $x = -20$ mm (x-rays outside the acryl phantom) to $x = 0$ mm (x-rays incident on the center of the acryl phantom) in steps of 0.5 mm. By using the axial symmetry of this phantom, the data from $+0.5$ to $+20$ mm were not measured but were constructed by reverse sorting of the order of the measured data set from $x = -20$ to $x = -0.5$ mm. The set of x-ray energy spectra for x-positions from -20 to $+20$ mm was repeated 60 times to obtain a rotational data set. This method greatly reduced the experimental time because each x-ray energy spectrum was measured with the

CZT detector for 900 s.

The x-scan results of the current measurement and FIX-ES measurement are shown in **Figs. 9** and **10**, respectively.

III. Results and Discussion

1. Simulation Study

According to the results of current measurement in the simulation calculation of the transmission image (Fig. 3), the effect of iodine contrast media decreases as the x-ray tube voltage and the diameter of the water phantom increase. This trend results from an increase in the relative number of high-energy x-rays due to the following beam hardening processes: (1) the increase in tube voltage brings an increase in the relative number of x-rays with higher energy that are less sensitive to absorption by iodine, and (2) as the water phantom becomes thicker, the number of x-rays with lower energy that are sensitive to absorption by iodine decreases because they become absorbed by the water.

As shown in Fig. 4, by comparison, the simulation calculation of FIX-ES measurement recorded the same change relative to the thickness of iodine regardless of tube voltage and water phantom thickness as predicted by Eq. (7). In Eq. (7), $\overline{\mu_I}(E_2)$ is greater than $\overline{\mu_I}(E_1)$, and $\overline{\mu_W}(E_2)$ is less than $\overline{\mu_W}(E_1)$: the attenuation coefficient of water in the energy range of approximately 33 keV monotonically decreases, while that of iodine drastically increases at the K-edge. As a result, the second and third terms of Eq. (7) are positive and negative, respectively. The relative $\ln(\phi_1/\phi_2)$ decreases as the water thickness increases, and it increases at the center of the phantom with the increasing thickness of iodine, as shown in Fig. 4.

In Fig. 6, CT images constructed by the current and FIX-ES measurement methods are shown for the iodine thickness of 60 µm in 10-mm-thick water layer. The CT images with lower iodine thickness are essentially the same as those in Fig. 6, with smaller CT values as shown in Fig. 7.

When the transmission images are converted to CT images, the advantage of FIX-ES measurement over current measurement becomes less obvious: logarithmic values of the transmission images are plotted in the CT images. The difference between air and water in the transmission images,
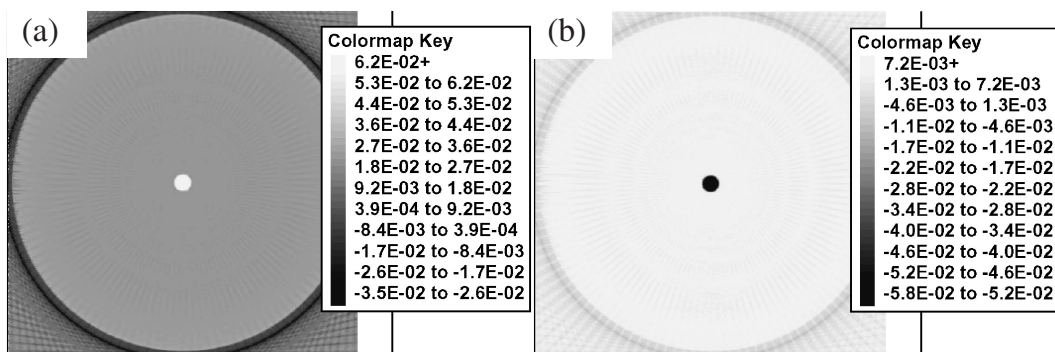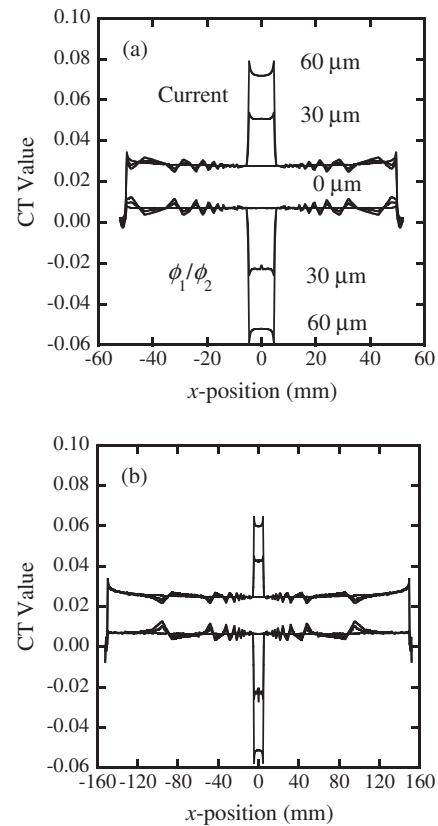
Fig. 6 CT images obtained by (a) current and (b) ϕ_1/ϕ_2 calculations for the case of an iodine thickness of 60 µm in 10-mm-thick water layer and water phantom of 200 mm diameter. The translation and rotation steps are 0.5 mm and 3°, respectively. The tube voltage and lanthanum filter thickness were 65 kV and 100 µm, respectively.
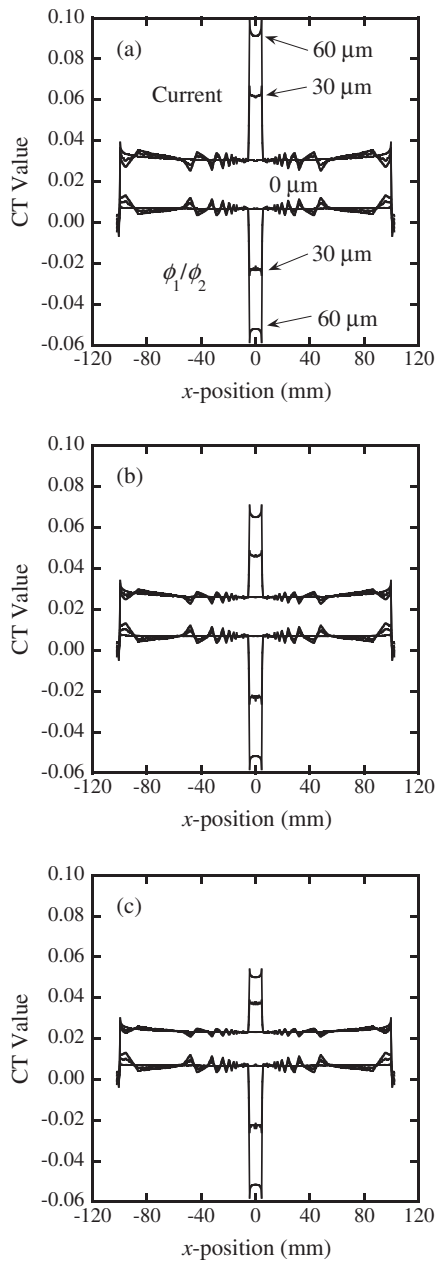
Fig. 7 CT values at the centers of CT images of Fig. 6. The x-ray tube voltages are (a) 50, (b) 65, and (c) 80 kV. The current and ϕ_1/ϕ_2 calculations are indicated in the figure. The iodine thickness in a 10-mm-thick water layer is shown in the figure.

Fig. 8 CT values as shown in Fig. 7, but with water phantom diameters of (a) 100 and (b) 300 mm. The x-ray tube voltage is 65 kV.

which is several orders of magnitude, appears as an offset in the CT values (Fig. 7); however, the CT images constructed using FIX-ES measurements, *i.e.*, ϕ_1/ϕ_2, have an advantage over those constructed by current measurements: the CT value in the iodine region is proportional to the iodine thickness, regardless of the x-ray tube voltage and the diameter of the phantom.

On the basis of the results shown in Figs. 3 and 4, we conclude that FIX-ES measurements have a marked advantage over current measurements in transmission radiography, especially in interventional radiology. Moreover, CT images constructed using the FIX-ES method, shown in Figs. 6 and 7, are free from x-ray beam hardening.

2. X-ray Transmission Measurements

The results of transmission measurements obtained using the current and FIX-ES methods are shown in Figs. 9 and 10, respectively. The results are plotted in the range of one decade, thereby enabling ready comparison with the results of the simulation study. The lines in the figures are smoothed lines of best fit.

The currents calculated using Eq. (8) were large numbers and errors were thus difficult to define. Moreover, the fluctuation of current is very small in practical current measurements. Considering the above, we neglected any errors in the current measurements. The experimental results showed the same trend with the simulation study, that is, the effect of iodine is greater when the x-ray tube voltage is lower. The slight advantage of using a lanthanum filter was observed.

In the FIX-ES method, the error increases with x-ray tube voltage; at a higher tube voltage, the number of x-rays with low energy, *i.e.*, around 30 keV, decreases and the statistical errors of ϕ_1 and ϕ_2 become greater in the measurements with the same measuring times as those for the lower tube voltage experiments. The peaks in the results for iodine of 60 μm thickness in a 10-mm-thick water layer shown in Fig. 10 are similar regardless of the tube voltage, as indicated in the simulation study. The results predicted by simulation study were thus examined in experiments.

From the comparison between Figs. 9 and 10, it was found that the current value in the acryl phantom region
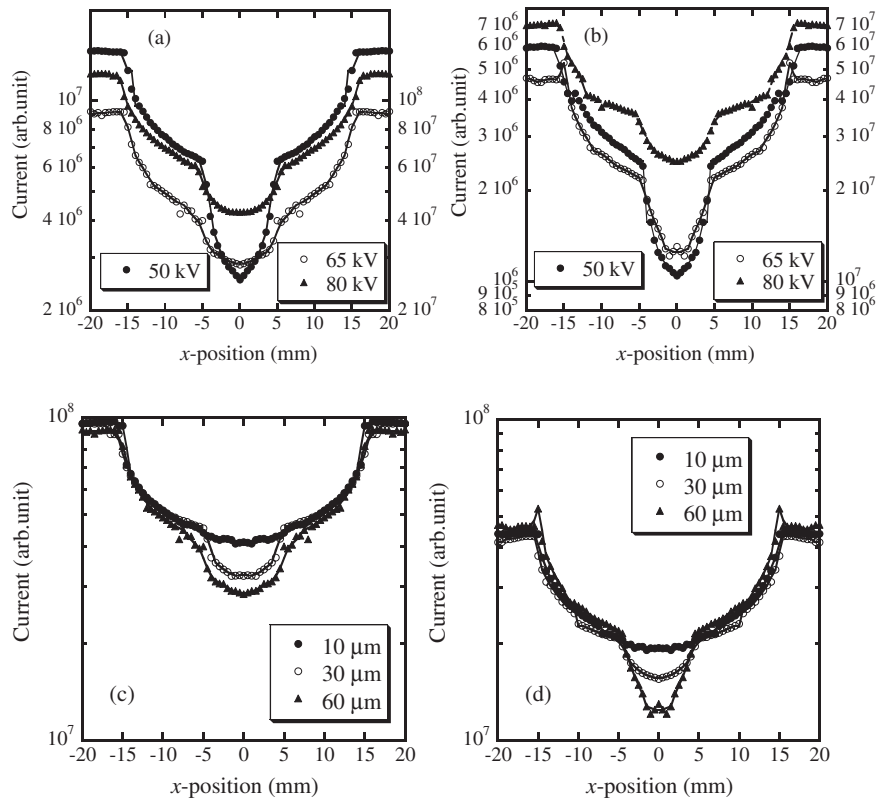
Fig. 9 Measured currents as a function of acryl phantom position for the case of an iodine thickness of 60 μm in a 10-mm-thick water layer (a) without and (b) with a 100-μm-thick lanthanum filter. The x-ray tube voltages are shown in the figures. Figures (c) and (d) show the measured currents obtained with a tube voltage of 65 kV without and with a 100-μm-thick lanthanum filter with different iodine thicknesses, respectively.
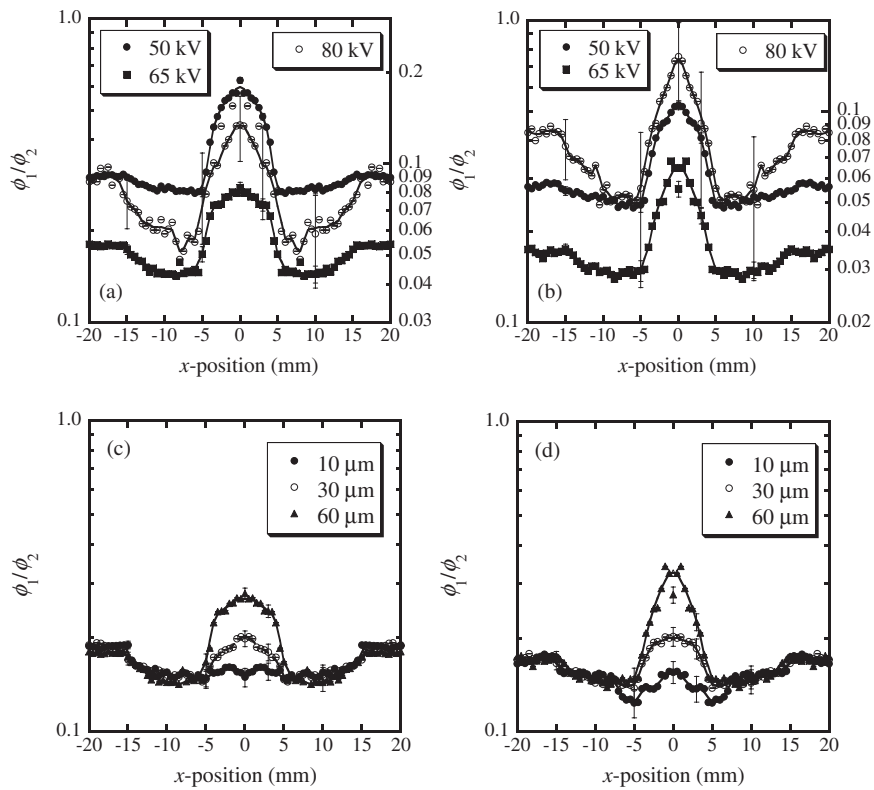
Fig. 10 FIX-ES measurements are shown under the same conditions as those in Fig. 9. Typical error bars are also shown.
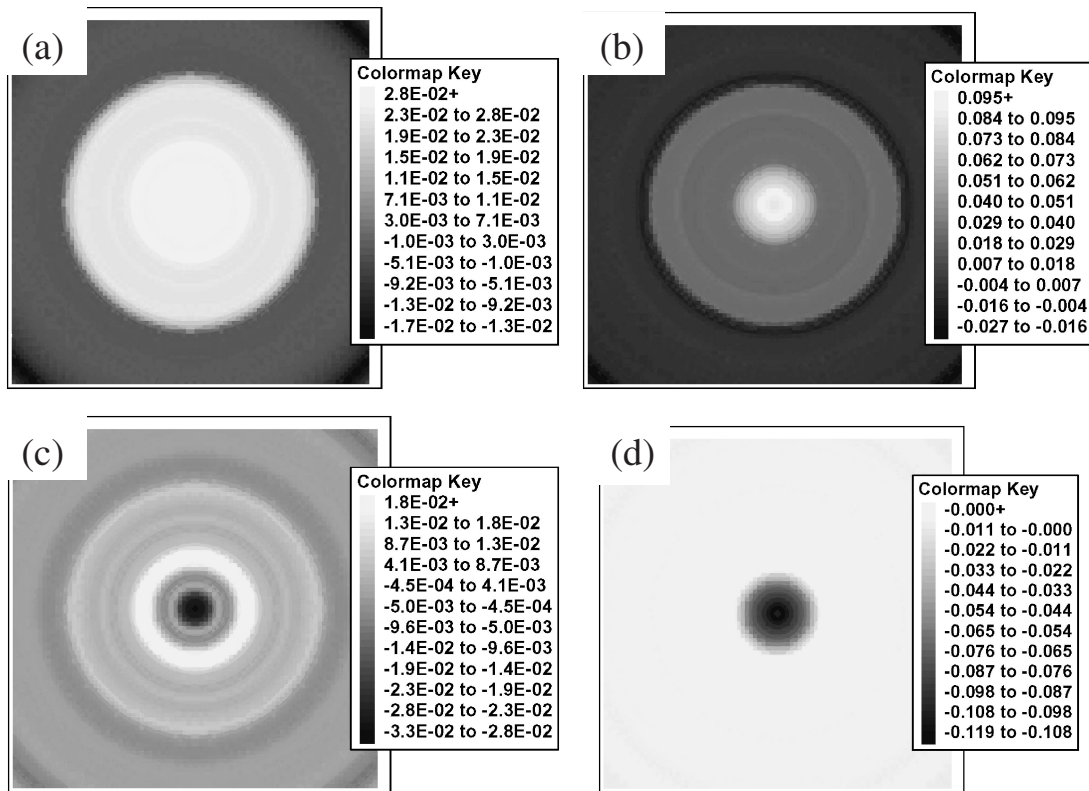
Fig. 11 CT images obtained by (a), (b) current and (c), (d) FIX-ES measurements for iodine thicknesses of (a), (c) 10 μm and (b), (d) 60 μm in a 10-mm-thick water layer, respectively, with a 100-μm-thick lanthanum filter. X-ray tube voltage was 65 kV.

changes much compared with the value of ϕ_1/ϕ_2. The change in current value is large with low x-ray tube voltage. The thickness change of the phantom was 30 mm maximum, while the summed thickness of the acryl and water phantoms was 230 mm. The effect of beam hardening is clearly observed in the current measurement even though the change in phantom thickness is 3/23. With high x-ray tube voltage, the change in ϕ_1/ϕ_2 value is observed in the acryl region. The reason for this change is not obvious; however, it might be attributed to the scattered x-rays.

A comparison of Figs. 10(c) and 10(d) reveals that the change in ϕ_1/ϕ_2 becomes more pronounced when a lanthanum filter is employed; this result was not predicted by the simulation study. Simplification in Eq. (7) neglected the effect of the lanthanum filter: with the change in x-ray spectrum due to the usage of the lanthanum filter, the averaged absorption coefficients of iodine in the two energy regions, however, change to some extent. When ϕ_2 is much greater than ϕ_1 in the filtered x-ray spectrum, which is obviously shown in Figs. 2 and 7 of Ref. 1), the second term of Eq. (7) becomes much greater, and the iodine region is observed more markedly. The factors that influence the use, and thus the effects, of the additional filter, *i.e.*, the material and its thickness, are worthy of future study.

3. Experimental CT Images

CT images were obtained using the smoothed lines of best fit shown in Figs. 9 and 10. The representative images shown in **Fig. 11** are based on (a), (b) current measurements

and (c), (d) FIX-ES measurements of 10 and 60 μm thicknesses of iodine with a lanthanum filter with tube voltage of 65 kV, respectively. In the current measurement, any change between the acryl and iodine regions is unremarkable. Particularly, detecting the iodine region of 10 μm thickness in 10-mm-thick water layer is very difficult in the current measurement, as shown in Fig. 11(a). In the FIX-ES measurement, however, only the iodine region is clearly observed on the CT image, although some fluctuations can be seen in Fig. 11(c). CT values are shown in **Figs. 12** and **13**, as quantitative estimation is difficult using CT images. In the current measurement, the CT value is greater for a lower tube voltage. By comparison, the valleys in the CT values in the FIX-ES measurement are nearly the same; however, they vary to a certain extent at the center of the phantom, and change is observed in the CT value (*i.e.*, the CT image) with fluctuations in the transmission measurements because of artifacts caused by the fluctuations of data. The advantage of using a lanthanum filter is slight but obvious in Fig. 12. However, by comparing iodine thicknesses at a tube voltage of 65 kV in Fig. 13, the iodine region of 10 μm thickness could be observed by FIX-ES measurement using a lanthanum filter. When the results of the current and FIX-ES measurements are compared in Fig. 13(b), the 10-μm-thick iodine region was observed by FIX-ES measurement but not by current measurement. We consider that an iodine thickness of 10 μm is the limit for detection when using the current measurement method.
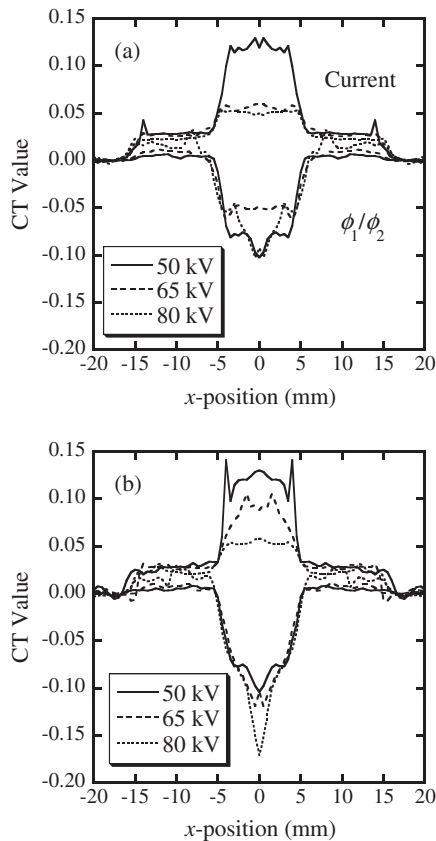
Fig. 12 CT values of CT images for current and FIX-ES measurements (a) without and (b) with a 100-μm-thick lanthanum filter in the case of an iodine thickness of 60 μm in a 10-mm-thick water layer. X-ray tube voltages are shown in the figure.

Fig. 13 CT values of CT images under the same conditions as those in Fig. 12, but for different iodine thicknesses. X-ray tube voltage was 65 kV.
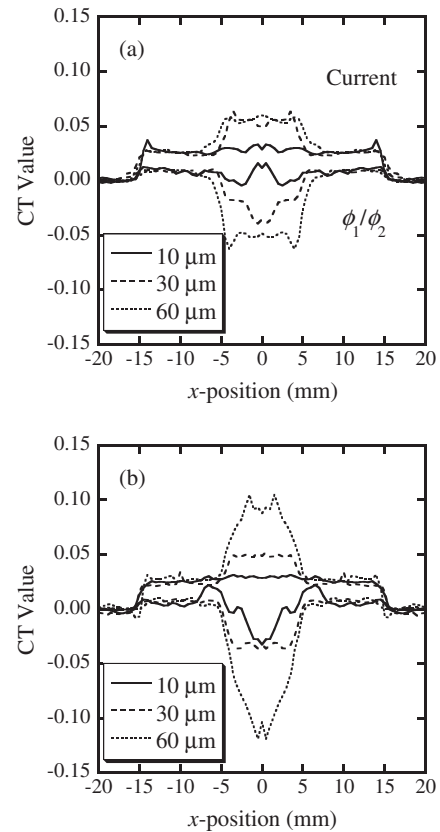
IV. Conclusions

A clear advantage exists for FIX-ES measurement over current measurement in transmission radiography and in CT. In the measurements performed in the present study, an iodine thickness of 10 μm in 10-mm-thick water layer was visualized by FIX-ES measurement but not by current measurement. The FIX-ES measurement method is independent of changes in x-ray tube voltage and phantom thickness: a cancer tissue could be observed in the same way regardless of the physical sizes of patients. This result will be of use in interventional radiology as well as transmission radiography and CT.

The simulation study demonstrated no obvious effect of the lanthanum filter in transmission measurements and the subsequent CT images; however, experiments indicated that the lanthanum filter is effective in detecting regions of iodine. Further study is warranted on the use of filters.

X-ray energy measurements should be performed at a high count rate for the practical application of the FIX-ES measurement method; this presents a challenge that remains for future radiation detector development.

Acknowledgements

The authors would like to express their thanks to Prof.

References

1) I. Kanno, S. Maetaki, H. Aoki, S. Nomiya, H. Onabe, "Low exposure x-ray transmission measurements for contrast media detection with filtered x-rays," *J. Nucl. Sci. Technol.*, **40**, 457 (2003).
2) I. Kanno, M. Takahashi, H. Aoki, H. Onabe, "Energy subtraction method with filtered x-rays for the detection of contrast media," *Nucl. Instrum. and Meth. in Phys. Res.*, **A567**, 154 (2006).
3) I. Kanno, A. Uesaka, S. Nomiya, H. Onabe, "Comparison of current and energy x-ray measurement methods in contrast media detection," *Nucl. Instrum. and Meth. in Phys. Res.*, **A580**, 534 (2007).
4) C. Sanders, M. S. Frank, G. T. Barnes *et al.*, "Metastatic calcification of the heart and lungs in end-stage renal disease: Detection and quantification by dual-energy digital chest radi-

ography," *AJR. Am. J. Roentgenol.*, **149**, 881 (1987).

5) S. E. Friedman, E. V. Dubovsky, J. Dubovsky *et al.*, "Mineral content of bone: Measurement by energy subtraction digital chest radiography," *AJR. Am. J. Roentgenol.*, **149**, 1199 (1987).

6) R. Kamimura, T. Takashima, "Single exposure energy subtraction chest radiography-Clinical survey of utility of bone image," *Nippon Acta Radiologica*, **49**, 562 (1989).

7) T. Katoh, "Quantitative image of bone mineral content-Dual energy subtraction in a single exposure," *Nippon Acta Radiologica*, **50**, 1127 (1990).

8) F. Toyofuku, K. Tokumori, "Monochromatic x-ray CT by synchrotron radiation," *Jpn. J. Radiol. Technol.*, **56**, 792 (2000).

9) H. Tsutsui, T. Ohtsuchi, K. Ohmori, S. Baba, "CdTe semiconductor x-ray imaging sensor and energy subtraction method

using x-ray energy information," *IEEE Trans. Nucl. Sci.*, **NS40**, 95 (1993).

10) T. Ohtsuchi, H. Tsutsui, K. Ohmori, S. Baba, "X-ray imaging sensor using CdTe crystals for dual energy x-ray absorptiometry," *IEEE Trans. Nucl. Sci.*, **NS41**, 1740 (1994).

11) Mallinckrodt Inc., "Optiray Pharmacy," MKR 13PB0806 (2006).

12) A. Maruhashi, K. Yamamoto, M. Matsumoto, private communications.

13) E. Storm, "Calculated bremsstrahlung spectra from thick tungsten targets," *Phys. Rev.*, **A5**, 2328 (1972).

14) M. Matsumoto, A. Yamamoto, I. Honda, A. Taniguchi, H. Kanamori, "Direct measurement of mammographic x-ray spectra using a CdZnTe detector," *Med. Phys.*, **27**, 1490 (2000).